Published in final edited form as:

Radiat Res. 2019 March ; 191(3): 278–294. doi:10.1667/RR15092.1.

Late Effects of ^{16}O Irradiation on Female Social and Cognitive Behavior and Hippocampal Physiology

Frederico Kiffer[a,b], **Tyler Alexander**[a,b], **Julie E. Anderson**[a,b], **Thomas Groves**[a,b,c], **Jing Wang**[a,b], **Vijayalakshmi Sridharan**[a,b], **Marjan Boerma**[a,b], **Antiño R. Allen**[a,b,c]

[a]Division of Radiation Health, University of Arkansas for Medical Sciences, Little Rock, AR 72205

[b]Department of Pharmaceutical Sciences, University of Arkansas for Medical Sciences, Little Rock, AR 72205

[c]Neurobiology & Developmental Sciences, University of Arkansas for Medical Sciences, Little Rock, AR 72205

Abstract

The radiation environment in space remains a major concern for manned space exploration, as there is currently no shielding material capable of fully protecting flight crews. Additionally, there is growing concern for astronauts' social and cognitive welfare, due to the prolonged radiation exposure and confinement they will experience on a mission to Mars. This study investigated the late effects of ^{16}O irradiation on social and cognitive behavior and neuronal morphology in the hippocampus of adult female mice. We gave 6-month-old mice whole-body exposure to ^{16}O at 0.25 or 0.1Gy (600 MeV/n; 18–33 cGy/min) at NASA's Space Radiation Laboratory in Upton, NY. Nine months following irradiation, animals underwent behavioral testing in the Three-Chamber Sociability and Novel Object Recognition and Y-maze paradigms. Exposure to 0.1 or 0.25 Gy ^{16}O significantly impaired object memory, a dosage of 0.25 Gy impaired social novelty learning, but neither dosage impaired short-term spatial memory. We observed significant decreases in mushroom spine density and dendrite morphology in the Dentate Gyrus, Cornu Ammonis 3, 2 and 1 of the hippocampus, which are consistent with key areas associated with object novelty and sociability processing. Our data suggest exposure to ^{16}O modulates hippocampal pyramidal and granular neurons and induces behavioral deficits at a time point of nine months after exposure in females.

Keywords

space; brain; neuron; morphology; radiation; Mars

*Address for corresponding author: Dr. Antiño R. Allen, University of Arkansas for Medical Sciences, 4301 West Markham, Suite 441B-2, Little Rock, AR 72205, Phone: 501-686-7553; Fax: 501-526-6599; Aallen@uams.edu.

Competing Interest: None of the authors has competing financial interests or other conflicts of interest.

INTRODUCTION

NASA's objective to safely carry humanity to Mars and back depends upon overcoming challenges associated with long-duration spaceflight. Flight crews will spend years in confinement, exposed to microgravity and the radiation environment of deep-space. Although the International Space Station has provided a wealth of data on the effects of microgravity on human health, its low Earth orbit is well within the planet's protective magnetosphere, thus limiting our knowledge of the effects of charged-particle radiation exposure on human health. NASA's current Mars Design Reference Architecture addendum indicates two possible orbital strategies beginning in the mid-2030s, one that ranges a round trip from 560–850 days, and one that ranges from 900–1,100 days.(1) The NASA-defined effective whole-body radiation dose equivalent for an 1,100 day mission is approximately 900 mSv, however the true dosage is dependent upon solar cycle activity.(2) Data collected from *Curiosity* in transfer to Mars and landed on the surface translates to a dose equivalent of 1.06 Sv for an estimated 850-day journey during solar maximum.(3, 4) Moreover, Building concern for astronaut cognitive welfare in-flight as well as upon return has led NASA to impose dosage limits for the central nervous system (CNS), which correspond specifically to the hippocampus. The lifetime CNS dose limit for all particles has been defined as 1.5 Gy. More specifically, for particles of $Z \geq 10$, the 1-year and career limitations are 0.1 and 0.25 Gy, respectively.(5)

The radiation environment in our solar system consists of high-energy charged nuclei expelled from dated supernovas, dubbed Galactic Cosmic Rays (GCR), which provide constant fluence, and from periodic Solar Particle Events (SPE) such as coronal mass ejections. Electromagnetic radiation, including X- and Gamma rays, is generally considered to be absorbed by spacecraft shielding, but there's currently no feasible shielding that is capable of fully mitigating the charged particles comprising GCR and SPE. The GCR spectrum consists of approximately 85% ^{1}H, 13% ^{2}He, and 1–2% energetic Z>2 (HZE) particles at median energies of 1,000 MeV/n.(6) Of the HZE spectra, ^{12}C and ^{16}O are found in highest abundance, and at the median energy of approximately 600 MeV/n.(7)

For now, space-radiation experiments are practically limited to ground-based simulations at NASA's Space Radiation Laboratory.(8) Recent rodent studies have demonstrated numerous behavioral deficits as a result of ^{16}O exposures at deep-space-relevant energies. Rats who received doses of 0.001 or 0.005 Gy (1,000 MeV/n) at 15 months of age showed anxiety via the Elevated Plus maze.(9) Mice who received 0.3 Gy (600 MeV/n) at 6 months failed to discriminate the novel object and object location via the Novel Object Recognition (NOR) and Object in Place paradigms.(10) Seven-week-old rats who received 0.01 or 0.05 Gy (600 MeV/n) failed to discriminate the novel object in the NOR.(11, 12) We've recently shown deficits in short-term memory via the Y-maze as a result of exposure to 0.5 Gy ^{1}H (150 MeV/n) followed shortly by 0.1 Gy ^{16}O (600 MeV/n) in six-month-old mice.(13)

Recent concern for the conditions flight crews will endure on a mission to Mars, have placed an impetus on the social dynamics astronauts will experience during their extended voyage. Whereas NASA and ESA have focused on long-term human group confinement studies such as HERA, SIRIUS, HI-SEAS, NEEMO, Antarctic outposts and others, recent findings that

charged-particle radiation appears to induce dendritic remodeling have led to the concern that social-processing circuits may also be affected as a result of radiation exposure, and may exacerbate the social challenges faced on a mission to Mars.(10, 13–18) Mange *et al* have recently shown social odor recognition deficits in male rats receiving 0.25 Gy ^{16}O (1,000 MeV/n) at one and six months post-exposure.(19) Krukowski *et al* have also shown social recognition deficits via the three-chamber sociability task in male mice 4 months after receiving 0.25 or 0.4 Gy ^{16}O (600 MeV/n).(20) Another recent study by the same group revealed social memory deficits in male mice 1.5–3 months after receiving 0.5 Gy of a mixed field of 60% ^{1}H (250 MeV/n), 20% ^{2}He (250 MeV/n) and ^{16}O (600 MeV/n), though female counterparts appeared to be spared from social memory deficits.(21)

The majority of studies pertaining to high-energy charged-particle radiation-induced cognitive insults, such as all of the aforementioned, are carried out in males, with few exceptions at this time.(21–24) Additionally, few studies have yet addressed radiation-induced changes to the CNS at a follow-up point of 9 months or longer.(17, 25–27) The present study explores changes in cognitive and social behaviors and hippocampal morphology of female mice nine months post-exposure to 0, 0.1 or 0.25 Gy of ^{16}O (600 MeV/n).

MATERIALS AND METHODS

Animals and Irradiation

Female C57BL/6 mice were purchased from Jackson Laboratory (Bar Harbor, ME). Five animals were housed per cage; they received standard low-soy rodent chow (2020X; Harlan® Laboratories Inc., Indianapolis, IN) and water *ad libitum* in 12:12 hour light-dark housing at the University of Arkansas for Medical Sciences (UAMS) in Little Rock, AR. Once animals reached six months of age, they were airlifted overnight to Brookhaven National Laboratory (BNL) in Upton, NY, where they received the same housing conditions. After acclimating for one week, animals received single, whole-body ^{16}O radiation at doses of 0, 0.1 or 0.25 Gy (600MeV/n, 18–33 cGy/min) at NASA's Space Radiation Laboratory (NSRL) within BNL. Mice were placed in well-ventilated acrylic cubes five at a time and mounted onto NSRL's foam holders prior to being placed on the beam line. Sham-irradiated animals were also placed on the beam line, but did not receive charged-particle radiation. Dosimetry was carried out by NSRL's physicists. Two days after irradiation, animals were airlifted back to UAMS, and followed a standard 8-week quarantine protocol consisting of 2020X chow containing 150ppm fenbendazole. All animal procedures were approved by the Institutional Animal Care and Use Committees of UAMS and BNL.

Y-Maze

Animal behavior was tested 9 months after irradiation (n=12 per radiation group). Mice were first tested in the Y-maze, which relies on neither negative nor positive reinforcement. The maze is constructed out of acrylic and consists of 3 similar arms (45 × 15 × 30 cm): a 'start' arm where animals are initially placed, a 'familiar' arm and a 'novel' arm. The familiar and novel arms each contain an object of different size and shape mounted at the end of the arm. Animals are placed facing away from the center of the maze in the 'start' arm. The

familiarization session consists of free exploration of the start and familiar arm. 4 hours later, animals were again placed in the maze, this time with access to all arms in the testing session. Allocation of arms (start, familiar, novel) was counterbalanced between within each experimental group. Trials lasted for 5 min, and center and nose-points were recorded throughout each session. All experimental arenas were wiped clean with 20% EtOH solution after each trial. All behavioral experiments were conducted during the light cycle under dimly-lit (white light) conditions, after one hour of acclimation. Behavioral experiments were also recorded on a charge-coupled device video camera, located above the mazes for automatic behavioral analysis with EthoVision® software version 11 (Noldus Information Technology).

Novel Object Recognition

Animals were next tested for NOR, a four-day procedure in which animals freely explore an arena for ten minutes each day. The first two days serve as habituation days, in which mice are able to explore an empty arena, effectively serving as an open field test; locomotor activity is measured at this stage. Familiarization occurs on day three, when animals explore the same arena containing two identical objects (cell-culture flasks filled with sand). Novel object recognition testing occurs on day four: One of the now-familiar objects is replaced by a novel object (large LEGO® blocks assembled to a similar size as the cell-culture flasks). (28) The arena is a cube consisting of an aluminum floor, acrylic walls (41 × 41 × 35 cm) and an open ceiling. Animals are placed in the center of the arena parallel to the objects, but placed in a randomized orientation to ensure no side bias. NOR testing relies on animals' endogenous propensity for exploring novelty in their environment; untreated animals will spend significantly more time exploring the novel object. The tracking software was programmed to track animal center points for the habituation trials and the nose-points during familiarization and testing trials. Animals who failed to explore the objects for a combination of < 10 visits were omitted from statistical analyses.

Three-Chamber Sociability

Next, mice underwent testing for social memory via the three-chamber sociability paradigm, in which mice freely explore three adjacent chambers for 10 minutes in three consecutive trials. The first trial consists of habituation, allowing mice to explore the 3 empty chambers. Trial 2 involves social familiarization, where a previously unknown animal (stimulus 1) of the same sex, strain, and age is placed in a small vertical cage on one of the lateral chambers, and the other lateral chamber contains an identical, but empty cage. For trial 3, another previously unknown animal (stimulus 2) of the same sex, strain, and age is placed in a small vertical cage on the opposite lateral chamber. Chamber selections for trials 2 and 3 are randomized to ensure there is no location bias. Strangers were randomly selected on a non-consecutive basis for each subject. Strangers were naïve animals housed in separate facilities and had no contact with test animals prior to behavioral testing, and were not aggressive. The apparatus is made of an aluminum floor, transparent acrylic walls, and an open ceiling. Each adjacent chamber has a dimension of (40 × 20 × 23 cm). Cages are made of aluminum and plastic. The tracking software was programmed to track animal nose-points during all trials.

Golgi Staining

The day after behavioral testing, animals were anesthetized with isoflurane, their brains were subsequently collected and dissected along the midsagittal plane. The Golgi method of staining has long proven to be a reliable method for assessing dendrite and dendritic spine dynamics due to various conditions, because of its resistance to fading or photobleaching over time.(29, 30) We adapted a staining protocol and used the reagents contained in the superGolgi kit (Bioenno Tech).(31) Right hemispheres were immediately impregnated in a potassium dichromate solution for two weeks (n = 5). Next, sections were immersed for at least 48 hours in a post-impregnation buffer. Samples were sectioned at 200 μm in 1X PBS along the coronal plane. Samples were then transferred into wells and washed with 0.01 M PBS buffer (pH 7.4) with Triton X-100 (0.3%) (PBS-T). Immediately after washing, samples were stained with ammonium hydroxide and then immersed in a post-staining buffer. Sections were again washed in PBS-T, mounted on 1% gelatin-coated slides, and allowed to dry. Sections were finally dehydrated with ethanol solutions, followed by cleaning in xylene, and coverslipped with Permount™ (Thermo Fisher Scientific).

Dendritic Morphology Quantification

All dendritic morphology data was collected blinded with regard to experimental conditions. We performed quantification of morphological characteristics of the granular and pyramidal neurons (n = 5 neurons per animal) contained in the hippocampal formation using techniques that included Sholl analyses, total dendritic length, number of branch points, and dendritic complexity index (DCI) using the Neuroexplorer component of the Neurolucida program. Sholl analysis is used to assess the amount and distribution of the arbor at increasing radial distances from the cell body.(32) Radii were set to extend in 10 μm intervals from the soma. The length of each dendritic branch, within each progressively larger circle, was counted from the soma, with respect to three dimensions. This provides information about the amount and distribution of individual dendrites.

We then performed branch-point analyses. Branch points occur at bifurcations of the dendrite when a branch divides into two sub-branches. Branch-point analysis depends on the number of bifurcations and the order of the points.(33) Lower branch-point orders represent proximal regions of the tree, whereas larger branch-point orders characterize distal regions. We used the branch-point analysis to determine the complexity of dendritic arborization, because the complexity of the dendritic tree is an important phenotypic component of branching analysis. DCI was determined by the following equation: DCI=∑(branch tip orders + # branch tips) × (total dendritic length/total number of primary dendrites). In the CA1, CA2, and CA3 areas, apical and basal dendrites were analyzed separately. We traced five randomly stained neurons per subregion per animal.

Dendritic Spine Density and Spine Morphology

We analyzed dendritic spines that were conducted on coded Golgi-impregnated brain sections that contained the dorsal and ventral hippocampus. Spines were examined on dendrites of the dorsal dentate gyrus (DG) granule neurons as well as apical (stratum radiatum) and basal (stratum oriens) dendrites of the dorsal CA1, CA2 and ventral CA3 pyramidal neurons. The neurons that satisfied the following criteria were chosen for analysis

in each of the experimental groups: 1) presence of non-truncated dendrites; 2) consistent and dark Golgi staining along the entire extent of the dendrites; and 3) relative isolation from neighboring neurons to avoid interference with analysis.(34) Five dendritic segments (each at least 20 nm in length) per neuron were analyzed, and 6–7 neurons were analyzed per brain.(35) Neurons that met staining criteria were traced using a 100 X oil objective, a computerized stage, and Neurolucida software (Ver. 11, Microbrightfield, Inc., Williston, VT).

Statistical Analyses

We expressed data as a mean ± the standard error of the mean (SEM). We analyzed the behavioral data throughout the length of each test. Y-maze exploration was analyzed by one-way analyses of variance (ANOVA). NOR visits were analyzed by paired *t*-tests, and habituation learning and habituation velocity by two-way mixed-factors ANOVA with post-hoc Holm-Sidak corrections for multiple comparisons. 3-Chamber Sociability exploration times were analyzed by one-way (ANOVA). Discrimination ratios (DR) were calculated by the following formulas: (*Y-Maze*) DR = (time spent exploring novel arm - time spent exploring familiar arm)/(time spent exploring novel arm + time spent exploring familiar arm); (*NOR*) DR = (novel object visits - familiar object visits)/(novel object visits + familiar object visits). We used ANOVA followed by a Bonferroni post-hoc test to evaluate statistical differences between sham and irradiated groups in measures of discrimination ratios, dendritic complexity index, and spine density. Sholl analyses were conducted via a mixed-factors ANOVA to test for effect of radiation on dendritic distance from the soma (the Sholl radius, being a repeated measures variable), with a Holm-Sidak post-hoc test, when appropriate. Dendritic spine data were compared via ANOVA with post-hoc Holm-Sidak corrections for multiple comparisons. All statistical analyses were conducted with GraphPad Prism 6.0 software (La Jolla, CA) in a 95% confidence interval, and $P < 0.05$ was considered significant.

RESULTS

Behavior

The Y-maze is an established behavioral assay for short-term spatial memory.(36) The amount of time a mouse spends exploring a novel arm relative to the familiar arm in the testing phase is indicative of its ability to retain the spatial memory encoded during familiarization. We observed that all irradiated groups displayed significant differences in exploration between the maze arms during the testing phase (0 Gy: $F_{(2, 33)} = 2.05$, $P < 0.01$; 0.1 Gy: $F_{(2, 33)} = 9.19$; $P < 0.001$; 0.25 Gy: $F_{(2, 33)} = 8.78$; $P < 0.001$). Post-hoc tests indicate that sham-irradiated animals spent significantly more time exploring the novel than the familiar ($P < 0.05$) or start ($P < 0.01$; Fig 1a) arms. Similarly, the 0.1 Gy group also spent significantly more time exploring the novel than familiar ($P < 0.01$) or start ($P < 0.001$; Fig 1b) arms. Finally, the group treated with 0.25 Gy was also successful in exploring the novel arm for longer periods of time than the familiar or start arms ($P < 0.01$; Fig 1c). Discrimination ratios provide a basis for interpreting animals' ability to remember a novel arm or object. A positive ratio can be interpreted as animals successfully discriminating between two objects, and a negative ratio implies 'forgetting' or failing to encode an object

in the first trial.(37) All cohorts showed positive discrimination ratios and there was no effect of radiation on discrimination ratios ($F_{(2, 32)} = 0.39$; $P = 0.68$; Fig 1d).

We used the NOR task to assess object recognition and spatial memory.(38, 39) Rodents naturally orient their head toward novel stimuli, behavior that provides a simple and effective method for quantifying recognition. Rodents display neophilia, and habituate to a stimulus with increased stimulus exposure; contrasting exploration of a novel versus a familiar object provides an index of object recognition and discrimination. Habituation learning occurs when animals' response to a stimulus lowers with increased exposure. Locomotor activity was tracked on the two empty arena habituation days, and the difference between total distances moved between open arena days 1 and 2 serve as a metric for habituation learning of the empty arena. We observed a significant interaction of time and radiation ($F_{(2, 22)} = 4.612$; $P < 0.05$) and a significant main effect of time on habituation learning ($F_{(1, 11)} = 26.44$; $P < 0.001$; Fig 2a). Post-hoc multiple comparisons show that the 0 and 0.25 Gy groups displayed habituation learning by significantly lowering exploration as a function of total distance moved on day two as compared to day one ($P < 0.001$) whereas the 0.1 Gy group showed no significant difference (Fig 2a). We also observed a significant interaction of time and radiation on velocity across the 4 days of NOR ($F_{(6, 66)} = 2.602$; $P < 0.05$), and a significant main effect of time on velocity ($F_{(3, 33)} = 46.58$; $P < 0.001$; Fig 2b). Post-Hoc multiple comparisons show a significant increase in velocity of mice receiving 0.1 Gy as compared to sham-irradiated animals ($P < 0.05$; Fig 2b) During familiarization (Day 3), mice were placed in the open field box with two identical objects. On day 4, one of the objects (henceforth 'familiar') was replaced with a novel object. Statistical analysis of total object visits in test sessions revealed exposure to 0.1 and 0.25 Gy ^{16}O significantly impaired mice; they did not show any preference for the novel object ($t = 0.21$, $P = 0.84$; Fig 2d; $t = 0.54$, $P = 0.59$; Fig 2e). Sham-irradiated mice showed novel object recognition and visited the novel object significantly more than the familiar object ($t = 4.13$, $P < 0.001$; Fig 2c). Radiation resulted in negative discrimination ratio for both groups ($F_{(2, 33)} = 2.66$; $P < 0.05$; Fig 2f).

Social behavior was assessed via the three-chamber test. All mice displayed normal habituation by spending approximately equal time exploring both lateral chambers ($F_{(5, 64)} = 0.82$; $P = 0.54$; Fig 3a). All experimental groups also socialized normally, by spending significantly more time exploring a stranger (stimulus 1) than an identical chamber with an empty cage during stage 2 ($F_{(5, 66)} = 11.42$; $P < 0.001$; Holm-Sidak multiple comparisons Stimulus vs Empty; O Gy $P < 0.05$; .1 Gy $P < 0.05$; .25 Gy $P < 0.01$ Fig 3b). Radiation affected social discrimination during the third stage in a dose-dependent manner, the higher dose eliciting an inability to discriminate between the familiar and stranger mouse, while sham and low-dose animals successfully spent more time exploring the novel stranger ($F_{(5, 65)} = 3.83$; $P = 0.004$; Holm-Sidak multiple comparisons Stimulus 1 vs Novel Stimulus; O Gy $P < 0.05$; .1 Gy $P < 0.05$; .25 Gy $P =$ NS Fig 3c).

Dendritic Morphology

Dentate Gyrus granule neurons.—We performed Sholl analyses to investigate the effects of ^{16}O on dendritic length as a function of increasing 10 μm intervals from the soma.

The effect of irradiation was found to be associated with a different distribution of dendritic branches over the entire tree in the Dentate Gyrus, as determined by ANOVA. We detected significant interactions between radiation and dendritic length at 0.1 Gy ($F_{(30,210)} = 7.69$; $P < 0.0001$) and 0.25 Gy ($F_{(30,240)} = 11.63$; $P < 0.0001$). We also found significant main effects of Sholl dendritic length after 0.1 Gy ($F_{(30,210)} = 32.28$; $P < 0.0001$) and 0.25 Gy ($F_{(30,240)} = 39.02$; $P < 0.0001$). We next performed post-hoc analyses, which revealed a decrease in the dendritic arbor significantly evident at 100 – 220 μm from the soma after 0.1 Gy (Holm-Sidak Multiple Comparisons: 80 – 100 μm and 220 μm, $P < 0.05$; 110 – 210 μm, $P < 0.001$; Fig 4a) and at 90 – 230 μm after 0.25 Gy (Holm-Sidak Multiple Comparisons: 90 – 100 μm, 220 – 230 μm, $P < 0.05$; 110 – 210 μm, $P < 0.0001$; Fig 4b).

In order to explore how different dosages affected the dendritic arbor, we performed Sholl analyses comparing the two radiation groups. We found no significant interactions between dosage and dendritic Sholl length ($F_{(30,210)} = 0.29$; $P > 0.99$; Fig. 4c). We next compared dendritic complexity in the DG between groups. An ANOVA found differences in dendritic complexity ($F_{(2, 11)} = 234.6$; $P < 0.0001$). Multiple comparisons show a marked decrease in complexity from Sham to 0.1 Gy ($P < 0.0001$) and from Sham to 0.25 Gy ($P < 0.0001$; Fig 4d). The variables that define dendritic complexity changed due to irradiation to similar extents as compared to sham. We observed decreases in dendritic length ($F_{(2,11)} = 74.66$; $P < 0.0001$), total bifurcations ($F_{(2,11)} = 122.7$; $P < 0.0001$), and dendritic ends ($F_{(2,11)} = 98.17$; $P < 0.0001$; see Table 1) in both dosage groups. Changes were localized to dendrites, as total cell area was not statistically different across cohorts ($F_{(2, 11)} = 0.21$; p = 0.81; see Table 1).

CA1 pyramidal neurons.—We next analyzed differences in the CA1 neurons between cohorts. We report significant interactions between radiation groups and dendritic Sholl length in the apical (0.1 Gy: $F_{(26,208)} = 10.43$; $P < 0.0001$; 0.25 Gy: $F_{(26,208)} = 9.827$; $P < 0.0001$) and basal (0.1 Gy: $F_{(20,160)} = 47.08$; $P < 0.0001$; 0.25 Gy: $F_{(19,152)} = 36.79$; $P < 0.0001$) subregions. Post-hoc multiple comparisons denoted significant dendritic length reductions at dosages of 0.1 Gy from 50 – 170 μm (Holm-Sidak Multiple Comparisons: 50 – 60 μm, $P < 0.05$; 70 – 170 μm, $P < 0.0001$; Fig 5a) and 0.25 Gy from 60 – 170 μm (Holm-Sidak Multiple Comparisons: 60 & 170 μm, $P < 0.05$; 70 – 160 μm, $P < 0.0001$; Fig 5c) from the soma in the apical CA1. The basal CA1 underwent similar changes, 0.1 Gy exposure resulted in dendrite decreases at 40 – 140 μm (Holm-Sidak Multiple Comparisons: 40 – 140 μm, $P < 0.001$; Fig 5b) and 0.25 Gy at 40 – 150 μm (Holm-Sidak Multiple Comparisons: 150 μm, $P < 0.05$; 40 – 140 μm, $P < 0.0001$; Fig 5d) from the soma.

In order to assess differences in dendritic reduction within the CA1, we compared dendritic length between irradiation groups. However, we noticed no significant changes in dendritic length between irradiated groups in the apical ($F_{(26,208)} = 0.21$, $P > 0.99$; Fig. 5e) and basal ($F_{(15,120)} = 1.21$, $P = 0.28$; Fig. 5f) CA1. Dendritic complexity appears to be severely reduced in response to ^{16}O at 0.1 and 0.25 Gy in the apical ($F_{(2, 12)} = 4.162$, $P < 0.0001$; Fig. 5g) and basal ($F_{(2, 12)} = 4.162$, $P < 0.0001$; Fig. 5h) subdivisions relative to sham. We observe that in the apical, CA1 irradiated groups underwent significant reductions in dendritic length ($F_{(2,12)} = 20.47$, $P < 0.0001$), total branch points ($F_{(2,12)} = 42.17$, $P < 0.0001$), and dendritic ends ($F_{(2,12)} = 36.22$, $P < 0.0001$; see Table 2) at both dosages.

Similarly, the basal CA1 underwent remodeling in consequence to radiation exposure to both dosages in measures of total dendrite length ($F_{(2,12)} = 37.33$, $P < 0.0001$), and branch points ($F_{(2,12)} = 101.9$, $P < 0.0001$), but we only saw changes in dendrite ends at 0.25 Gy ($F_{(2,12)} = 117.9$, $P < 0.0001$; see Table 2).

CA2 pyramidal neurons.—Our next step was to examine changes in dendritic length due to radiation in the CA2. Two-way ANOVA showed significant interactions between radiation and Sholl dendrite length in the apical (0.1 Gy: $F_{(24,192)} = 2.01$, $P < 0.01$; 0.25 Gy: $F_{(24,192)} = 5.44$, $P < 0.0001$) and basal (0.1 Gy: $F_{(20,160)} = 5.31$, $P < 0.0001$; 0.25 Gy: $F_{(20,160)} = 25.64$, $P < 0.0001$) regions. Post-hoc analyses revealed significant dendritic reductions at different dosages: 0.1 Gy exposure resulted in significantly shorter dendrites at 140 – 170 μm (Holm-Sidak Multiple Comparisons: 140 – 160 μm, $P < 0.01$; 160 – 170 μm, $P < 0.05$; Fig 6a) from the soma within the apical region, and at 90 – 150 μm (Holm-Sidak Multiple Comparisons: 90 μm, $P < 0.05$; 150 μm, $P < 0.05$; 100 – 140 μm, $P < 0.0001$; Fig 6b) from the soma in the basal region of the CA2. Irradiation at 0.25 Gy also induced dendritic Sholl length reduction at 120 – 200 μm (Holm-Sidak Multiple Comparisons: 120, 150–160 μm, $P < 0.01$; 100 – 140 μm, $P < 0.0001$; Fig 6c) in the apical division and in the basal at 50 – 150 μm (Holm-Sidak Multiple Comparisons: 150 μm, $P < 0.05$; 50 – 140 μm, $P < 0.0001$; Fig 6d) from the soma. In order to compare dosage-dependent changes due to ^{16}O we ran two-way ANOVA between irradiation groups. We did not observe interactions between cohorts and dendritic length in the apical CA2 ($F_{(24,192)} = 0.69$, $P = 0.86$; Fig. 6e). However, we detected significant interactions between dendritic length in irradiated groups in the basal CA2 ($F_{(20,160)} = 16.30$, $P < 0.0001$). Multiple comparisons reveal that the 0.25 Gy cohort had significantly reduced dendritic length in the basal CA2 at 50 – 120 μm compared to the 0.1 Gy group (Fisher's LSD: 50, 120 μm, $P < 0.05$; 60 – 110 μm, $P < 0.0001$; Fig 6f). Apical complexity within the CA2 appears to have been significantly reduced in response to irradiation ($F_{(2, 12)} = 10.81$, $P < 0.01$) at both dosages (0.1 Gy, 0.25 Gy, $P < 0.01$; Fig 6g). However, 0.25 Gy was the only dosage to result in decreased dendrite complexity in the basal CA2 ($P < 0.001$; Fig 6h). Our measurements of dendritic length, branch points and dendritic ends were consistent with the dendritic complexity index. Apical dendrites showed significantly reduced total length ($F_{(2, 12)} = 21.61$, $P < 0.0001$), bifurcations ($F_{(2, 9)} = 63.07$, $P < 0.0001$) and dendrite ends ($F_{(2, 9)} = 66.90$, $P < 0.0001$; see Table 3) in both radiation groups in comparison to sham. In line, the basal CA2 showed decreased branch points ($F_{(2,11)} = 26.08$, $P < 0.0001$) and dendrite ends ($F_{(2, 12)} = 19.11$, $P < 0.001$) only at 0.25 Gy, with the exception of total dendritic length, which was reduced at both dosages, with dose dependence ($F_{(2, 10)} = 58.84$, $P < 0.0001$; see Table 3). We noticed no changes in cell area across cohorts ($F_{(2, 11)} = 1.20$, $P = 0.34$; see Table 3).

CA3 pyramidal neurons.—Finally, we conducted Sholl analyses in the hippocampal CA3. We found significant interactions between irradiation and segmental dendritic Sholl length in both dosages at the apical (0.1 Gy: $F_{(24,192)} = 4.49$, $P < 0.0001$; 0.25 Gy: $F_{(24,192)} = 5.53$, $P < 0.0001$) and basal (0.1 Gy: $F_{(24,192)} = 3.56$, $P < 0.0001$; 0.25 Gy: $F_{(24,192)} = 4.59$, $P < 0.0001$) CA3. Within the apical CA3, we observed a significant reduction in dendritic length due to 0.1 Gy at distances of 110 – 160 μm from the soma (Holm-Sidak Multiple Comparisons: 110 μm $P < 0.01$, 160 μm, $P < 0.05$; 120 – 150 μm, $P < 0.001$; Fig

7a). A dosage of 0.25 Gy also induced reductions in dendritic length at 110 – 180 μm, from the soma (Holm-Sidak Multiple Comparisons: 110–160 μm, $P < 0.0001$; 170 μm, $P < 0.001$; 180 μm P < 0.01; Fig 7c) when compared to sham. We observed similar changes in the basal CA3. A dosage of 0.1 Gy induced dendritic reductions at 100 – 160 μm from the soma (Holm-Sidak Multiple Comparisons: 100–110, 140–160 μm, $P < 0.05$; 120 – 170 μm, $P < 0.0001$; Fig 7b), and a dosage of 0.25 Gy resulted in reduced dendritic length at distances of 70 – 170 μm from the soma (Holm-Sidak Multiple Comparisons: 100, 140–160 μm, $P < 0.05$; 120 – 170 μm, $P < 0.0001$; Fig 7d) relative to sham. We then assessed differences in dendritic shortening due to radiation dosage. We saw no significant interactions between dosage and dendritic length in the apical ($F_{(24,192)} = 0.23$, $P > 0.99$; Fig. 7e) nor basal ($F_{(24,192)} = 0.49$, $P = 0.98$; Fig. 7f) CA3. We then measured differences in dendritic complexity across cohorts. We observed no changes in the apical CA3 ($F_{(2, 12)} = 2.30$, $P = 0.14$; Fig 7g). This was despite observing changes in individual complexity parameters within the apical CA3, such as total dendritic length ($F_{(2, 11)} = 16.42$, $P < 0.001$), branch points ($F_{(2, 12)} = 5.47$, $P < 0.05$) and dendritic ends ($F_{(2, 11)} = 16.42$, $P < 001$; see Table 4) However, we noticed a significant decrease in the basal CA3 ($F_{(2, 12)} = 7.96$, $P < 0.01$) dendrite complexity, but multiple comparisons show significance only at the higher dosage of 0.25 Gy ($P < 0.05$; Fig 7h). We noticed significant changes in total dendritic length ($F_{(2, 12)} = 7.34$, $P < 0.01$) and branch points ($F_{(2, 11)} = 8.83$, $P < 0.01$) in the basal CA2 at both radiation dosages, but we only detected changes in dendritic ends at 0.25 Gy ($F_{(2, 12)} = 4.63$, $P < 0.01$; see Table 4).

Spine Morphology

To further investigate the effects of ^{16}O on hippocampal physiology, we performed spine-density analyses between cohorts. The DG showed that radiation had a significant effect on mushroom-spine density ($F_{(2, 33)} = 2.59$, $P < 0.001$). Post-hoc analysis revealed reductions in mushroom-spine density were significant for both dosages (Sham vs. 0.1 Gy, $P < 0.001$; Sham vs. 0.25 Gy, $P < 0.001$; Fig 8a). We also found an effect of radiation on the apical ($F_{(2, 12)} = 2.9$, $P < 0.01$) and basal ($F_{(2, 14)} = 0.23$, $P < 0.0001$) CA1 mushroom spines. Post-hoc analyses revealed dose-dependent decreases in mushroom-spine density in both the apical (Sham vs. 0.1 Gy, $P < 0.05$; Sham vs. 0.25 Gy, $P < 0.01$; Fig 8b) and basal (Sham vs. 0.1 Gy, $P < 0.001$; Sham vs. 0.25 Gy, $P < 0.0001$; Fig 8c). Similarly to the CA 1, the CA2 was also found to have reduced mushroom-spine density in the apical CA2 at both dosages (Sham vs. 0.1 Gy, $P < 0.05$; Sham vs. 0.25 Gy, $P < 0.05$; Fig 8d) and in the basal CA2 at 0.25 Gy ($P < 0.05$; Fig 8e). The basal CA2 was also found to have had an effect of radiation on total spine density ($F_{(2, 14)} = 2.29$, $P < 0.01$), yet the decrease was statistically significant only when comparing Sham to 0.25 Gy-irradiated cohorts. Finally, we also found an effect of radiation on the apical ($F_{(2, 12)} = 8.61$, $P < 0.01$) and basal ($F_{(2, 14)} = 19.71$, $P < 0.0001$) CA3 mushroom spines. Post-hoc analyses revealed dose-dependent decreases in mushroom-spine density in both the apical (Sham vs. 0.1 Gy, P < 0.05; Sham vs. 0.25 Gy, P < 0.01; Fig 8f) and basal (Sham vs. 0.1 Gy, P < 0.001; Sham vs. 0.25 Gy, P < 0.0001; Fig 8g).

DISCUSSION

The current study addresses changes ^{16}O induces in the hippocampus of female mice nine months post-exposure. We found that radiation at 0.1 Gy and 0.25 Gy induced deficits in object memory. Additionally, we observed that radiation induced deficits in social novelty only at a higher dosage of 0.25 Gy. However, we observed no changes in short-term spatial memory. Furthermore, we found that radiation at both dosages induced hippocampus-wide changes to dendrite morphology. The DG underwent significant reductions in dendritic length and complexity, as well as reductions in mushroom-spine density. We observed minor, but significant, dendrite reductions in the ventral CA3, though dendrite complexity was reduced significantly only in the basal CA3 at 0.25 Gy. The dorsal CA2 was observed to undergo significant dendrite reductions at both dosages, accompanied by significant reductions in apical dendritic complexity across treated cohorts, but only in animals treated with 0.25 Gy in the basal CA2, with an identical pattern in mushroom-spine density in the apical and basal subregions. Finally, the dendrites of the apical and basal CA1 were shorter in irradiated animals. Dorsal CA1 dendrite complexity was markedly lower at both dosages; radiation reduced mushroom-spine density in a dose-dependent fashion.

Deficits in object recognition memory have been previously observed in rodents treated with several different particles. ^{1}H exposure induced NOR deficits in mice one month after receiving 0.5 or 2 Gy, and in mice three months after receiving 0.1 Gy.(40, 41) ^{2}He exposure compromised recognition memory in mice receiving 0.15 and 0.5 Gy.(42) Exposure to HZE particles also induces NOR deficits. Mice given 0.3 Gy of ^{16}O, 0.3 or 0.05 Gy of ^{48}Ti failed to recognize a novel object six weeks after exposure.(10, 15) 0.25 Gy of ^{56}Fe and 0.05 Gy of ^{16}O resulted in an inability of rats to distinguish the novel object immediately after irradiation.(11) There are inherent sex differences in hippocampus structure and function.(43–45) Yet, the only other studies that address female NOR performance after charged-particle irradiation have found that two weeks after exposure to 0.1, 0.2 or 0.5 Gy of ^{56}Fe (600 MeV/n), males and females showed equal deficits, and mice receiving high doses of ^{56}Fe (1–3 Gy) showed minor sex differences in deficits, with females failing to discriminate the novel object at 3 Gy and males at 2 Gy.(24, 46) A more recent low-dose study found 0.15 or 0.5 Gy of ^{1}H + ^{2}He + ^{16}O elicited recognition memory deficits in males, but not females 80–100 days following radiation.(21) Our findings are generally consistent with other single-particle studies, and suggest that recognition memory deficits at low doses in females may occur only at late time points.

NOR is considered a hippocampus-dependent task.(38) The dorsal hippocampus in particular is implicated in novel-object signaling. Within the dorsal hippocampus, the CA1 is paramount for object-novelty processing, as it is the main hippocampal output of the tri-synaptic pathway, and broadcasts environmental novelty.(47) Environmental novelty signaling is accomplished by the modulation of fast-gamma oscillations within place cells, which occur with CA3-CA1 phase synchrony during novelty exploration.(48) We observed dose-independent reductions in the apical and basal dendrites of the dorsal CA1, accompanied by severe reductions in dendrite complexity. We observed similar changes to the dorsal DG. Both hippocampal regions were found to undergo reductions in mushroom-spine density. Mushroom spines are the most stable synaptic sites along a dendrite,

providing stable synaptosomes that persist for long durations.(49) Additionally, dendrites and axons must reach input and output targets respectively, for targeted network processing.(50) Previous studies have shown dendritic spine modulation in response to various particle exposures, and in particular, a general decrease in mushroom spine density in the prefrontal cortex and hippocampus.(10, 13–15, 17, 18) The reductions in mushroom spines and dendritic length observed in the DG and CA1 of irradiated animals suggest severe circuit input and output modulation, which may have affected object processing.

The three-chamber sociability paradigm was conceived and established by Dr. Jaqueline Crawley as a means to quantify autistic-like behavior in mouse models of Autism Spectrum Disorders (ASD).(51) Although this test condition has been widely adopted in ASD research, three-chamber sociability deficits have also been observed in mice undergoing cocaine withdrawal, models of schizophrenia, and neonatal *status epilepticus*.(52–54) We found that mice who received 0.25 Gy failed to discriminate between a stranger and a familiarized mouse, but showed profound discrimination between an empty cage and a stranger mouse.

There is ongoing debate as to what hippocampal subregion is responsible for social processing in rodents. Felix-Ortiz and Tye have demonstrated that optogenetic modulation of basolateral amygdala projections to the ventral hippocampus directly modulates three-chamber sociability and resident-intruder social behaviors.(55) However, Hitti and Siegelbaum have demonstrated that transgenic mice with inactivated dorsal hippocampal CA2 pyramidal neurons showed profound deficits in social novelty, as determined by the three-chamber sociability paradigm, but retained novel-object recognition, a dorsal hippocampus-dependent task, and contextual fear memory, a ventral hippocampus-dependent task. Furthermore, Hitti and Siegelbaum observed deficits in social memory via the direct interaction and 5-trial social memory assays. The authors suggest a role in the dorsal CA2 for non-spatial hippocampal tasks, which likely does not involve the classic tri-synaptic pathway, but instead may include novel direct input projections the authors identified from the lateral entorhinal cortex, median raphe nucleus, and hypothalamic supramammillary nucleus.(56) Our observation of the degree to which arborization decreased in the dorsal CA2 appears to be consistent with Hitti and Siegelbaum's findings. We observed a more-pronounced reduction in dendritic length, complexity, and mushroom spine density within the 0.25 Gy group, which coincides with the observed social novelty deficits seen this group, but not in the 0.1 Gy group. In particular, these dosage-dependent differences occurred within the basal, but not apical CA2.

The ventral CA3 has also been recently implicated in social recognition memory. Chiang *et al* have found that the ventral CA3 plays a critical role in encoding social stimuli. Furthermore, inactivation of the ventral CA3 results in social novelty deficits as assessed by three-chamber sociability.(57) The morphological changes we observed in the CA3 suggests that the ventral hippocampus was not immune to radiation-induced dendrite dysmorphia, and although dendrite reductions were not as pronounced, they likely played a detrimental role in social novelty processing. Interestingly, some CA2 pyramidal neurons project to and from the ventral CA3 in a mutually inhibitory loop, suggesting a potential crosstalk in social

processing between the hippocampal subunits, though much work is needed to elucidate social processing circuits.(58, 59)

Our findings are strikingly consistent with the work by Mange *et al*, who recently showed that male rats irradiated with ^{16}O at 0.25 Gy (1,000 MeV/n) failed to discriminate exploration of a novel social odor bead during the recognition phase of the Social Odor Recognition paradigm at six months after irradiation, whereas rats irradiated at 0.05 Gy were unaffected. The authors also observed that the proliferating cells of the subventricular zone remained unaffected by radiation, and suggest that the observed socio-cognitive deficits were likely not due to olfactory sensory injury.(19) Our data validates the long-term social memory deficit results obtained by Mange *et al* and suggests social odor, regardless of animal presence is the driving factor in rodent short-term social memory. Kurkowsky *et al* recently report that female mice are spared from social memory deficits 1.5–3 months following exposure to $^{1}H + ^{2}He + ^{16}O$.(21) The dosage contribution from ^{16}O alone in the study was approximately 0.1 Gy-which in our study was insufficient to result in social memory deficits. It's possible that within females, social memory impairments may be under a separate dose-dependence from males, but may not necessarily be spared from maladaptive responses to radiation.

The rodent olfactory tract begins at the olfactory epithelium and vomeronasal organ, which project to the main and accessory olfactory bulbs. From there, information is relayed to the anterior olfactory nucleus and piriform cortex, before projecting to the amygdala.(60, 61) The amygdala innervates the lateral septum, which in turn projects to and from the ventral hippocampus.(62) The amygdala also projects to the entorhinal cortex, to which the hippocampal CA2 also relays. Recent work by Dias *et al* highlights a crucial synergistic role between the medial amygdala and hippocampus in long-term social memory contextual cue processing. The authors also emphasize the role of the CA2 in long-term social memory, and suggest the CA2 is crucial for the early consolidation phase of social memory formation.(63)

CONCLUSION

Exposure to ^{16}O induced deficits in NOR at 0.1 Gy and 0.25 Gy, and in sociability only in mice treated with 0.25 Gy. We observed reductions to the dendritic arbor and dendritic spines which appear to support to the behavioral deficits. These data suggest novel concern for long-term female astronaut welfare after charged-particle radiation exposure. Future work should explore sociability in females at earlier time points and a wider range of dosages. As social-processing circuits are determined, electrophysiological work should be performed to address specific hippocampal vulnerabilites to charged-particle radiation. More attention should be placed on mechanisms of dendrite dysmorphia at discrete hippocampal subregions. Finally, future work should explore how radiation-induced social memory deficits in rodents can translate to human social dynamics in the context of long-duration spaceflight.

Acknowledgements:

We thank Mr. Jarod Daily and the UAMS science communication group for grammatical editing of this manuscript.

Funding: This work was supported by the National Space Biomedical Research Institute (NSBRI) Grant RE03701 through NASA cooperative agreement NCC 9-58. This work was also supported by Core Facilities of the Center for Translational Neuroscience IDeA program award P30 GM110702. The funders had no role in study design, data collection and analysis, decision to publish, or preparation of the manuscript.

References

1. Human Exploration of Mars Design Reference Architecture 5.0 Addendum #2. 2014.
2. National Research Council (U.S.). Committee for Evaluation of Space Radiation Cancer Risk Model., National Research Council (U.S.). Space Studies Board Technical evaluation of the NASA model for cancer risk to astronauts due to space radiation. Washington, D.C.: National Academies Press; 2012 x, 75 p. p.
3. Zeitlin C, Hassler DM, Cucinotta FA, Ehresmann B, Wimmer-Schweingruber RF, Brinza DE, et al. Measurements of energetic particle radiation in transit to Mars on the Mars Science Laboratory. Science. 2013;340(6136):1080–4. Epub 2013/06/01. [PubMed: 23723233]
4. Hassler DM, Zeitlin C, Wimmer-Schweingruber RF, Ehresmann B, Rafkin S, Eigenbrode JL, et al. Mars' surface radiation environment measured with the Mars Science Laboratory's Curiosity rover. Science. 2014;343(6169):1244797 Epub 2013/12/11. [PubMed: 24324275]
5. Nelson GA, Simonsen L, Huff JL. NASA Evidence Report: Risk of Acute and Late Central Nervous System Effects from Radiation Exposure. 2016.
6. Nelson GA. Space Radiation and Human Exposures, A Primer. Radiation research. 2016;185(4):349–58. Epub 2016/03/29. [PubMed: 27018778]
7. George JS, Lave KA, Wiedenbeck ME, Binns WR, Cummings AC, Davis AJ, et al. Elemental Composition and Energy Spectra of Galactic Cosmic Rays during Solar Cycle 23. Astrophys J. 2009;698(2):1666–81.
8. La Tessa C, Sivertz M, Chiang IH, Lowenstein D, Rusek A. Overview of the NASA space radiation laboratory. Life sciences in space research. 2016;11:18–23. Epub 2016/12/21. [PubMed: 27993189]
9. Rabin BM, Carrihill-Knoll KL, Miller MG, Shukitt-Hale B. Age as a factor in the responsiveness of the organism to the disruption of cognitive performance by exposure to HZE particles differing in linear energy transfer. Life sciences in space research. 2018;16:84–92. Epub 2018/02/25. [PubMed: 29475524]
10. Parihar VK, Allen B, Tran KK, Macaraeg TG, Chu EM, Kwok SF, et al. What happens to your brain on the way to Mars. Science advances. 2015;1(4). Epub 2015/07/17.
11. Rabin BM, Poulose SM, Carrihill-Knoll KL, Ramirez F, Bielinski DF, Heroux N, et al. Acute Effects of Exposure to (56)Fe and (16)O Particles on Learning and Memory. Radiation research. 2015;184(2):143–50. Epub 2015/07/25. [PubMed: 26207687]
12. Rabin BM, Shukitt-Hale B, Carrihill-Knoll KL, Gomes SM. Comparison of the effects of partial- or whole-body exposures to (1)(6)O particles on cognitive performance in rats. Radiation research. 2014;181(3):251–7. Epub 2014/03/13. [PubMed: 24611658]
13. Kiffer F, Carr H, Groves T, Anderson JE, Alexander T, Wang J, et al. Effects of (1)H + (16)O Charged Particle Irradiation on Short-Term Memory and Hippocampal Physiology in a Murine Model. Radiation research. 2018;189(1):53–63. Epub 2017/11/15. [PubMed: 29136391]
14. Allen AR, Raber J, Chakraborti A, Sharma S, Fike JR. (56)Fe Irradiation Alters Spine Density and Dendritic Complexity in the Mouse Hippocampus. Radiation research. 2015;184(6):586–94. Epub 2015/11/19. [PubMed: 26579941]
15. Parihar VK, Allen BD, Caressi C, Kwok S, Chu E, Tran KK, et al. Cosmic radiation exposure and persistent cognitive dysfunction. Scientific reports. 2016;6:34774 Epub 2016/10/11. [PubMed: 27721383]
16. Kiffer F, Howe A, Carr H, Wang J, Alexander T, Anderson JE, Groves T, Seawright J, Sridharan V, Carter G, Boerma M, Allen AR. Late Effects of ^{1}H irradiation on hippocampal physiology. Life Sciences in Space Research. 2018;17:51–62. [PubMed: 29753414]
17. Kiffer F, Howe AK, Carr H, Wang J, Alexander T, Anderson JE, et al. Late effects of (1)H irradiation on hippocampal physiology. Life Sci Space Res (Amst). 2018;17:51–62. Epub 2018/05/14. [PubMed: 29753414]

18. Carr H, Alexander TC, Groves T, Kiffer F, Wang J, Price E, et al. Early effects of (16)O radiation on neuronal morphology and cognition in a murine model. Life Sci Space Res (Amst). 2018;17:63–73. Epub 2018/05/14. [PubMed: 29753415]
19. Mange A, Cao Y, Zhang S, Hienz RD, Davis CM. Whole-Body Oxygen ((16)O) Ion-Exposure-Induced Impairments in Social Odor Recognition Memory in Rats are Dose and Time Dependent. Radiation research. 2018;189(3):292–9. Epub 2018/01/16. [PubMed: 29332539]
20. Krukowski K, Jones T, Campbell-Beachler M, Nelson G, Rosi S. Peripheral T Cells as a Biomarker for Oxygen-Ion-Radiation-Induced Social Impairments. Radiation research. 2018;190(2):186–93. Epub 2018/05/29. [PubMed: 29809107]
21. Krukowski K, Grue K, Frias ES, Pietrykowski J, Jones T, Nelson G, et al. Female mice are protected from space radiation-induced maladaptive responses. Brain, behavior, and immunity. 2018 Epub 2018/08/15.
22. Whoolery CW, Walker AK, Richardson DR, Lucero MJ, Reynolds RP, Beddow DH, et al. Whole-Body Exposure to (28)Si-Radiation Dose-Dependently Disrupts Dentate Gyrus Neurogenesis and Proliferation in the Short Term and New Neuron Survival and Contextual Fear Conditioning in the Long Term. Radiation research. 2017;188(5):532–51. Epub 2017/09/26. [PubMed: 28945526]
23. Sweet TB, Panda N, Hein AM, Das SL, Hurley SD, Olschowka JA, et al. Central nervous system effects of whole-body proton irradiation. Radiation research. 2014;182(1):18–34. Epub 2014/06/18. [PubMed: 24937778]
24. Haley GE, Yeiser L, Olsen RH, Davis MJ, Johnson LA, Raber J. Early effects of whole-body (56)Fe irradiation on hippocampal function in C57BL/6J mice. Radiation research. 2013;179(5):590–6. Epub 2013/03/21. [PubMed: 23510274]
25. Rabin BM, Carrihill-Knoll KL, Carey A, Shukitt-Hale B, Joseph JA. Effect of diet on the disruption of operant responding at different ages following exposure to (56)Fe particles. Age. 2005;27(1):69–73. Epub 2005/03/01. [PubMed: 23598605]
26. Villasana LE, Benice TS, Raber J. Long-term effects of 56Fe irradiation on spatial memory of mice: role of sex and apolipoprotein E isoform. International journal of radiation oncology, biology, physics. 2011;80(2):567–73. Epub 2011/05/10.
27. Parihar VK, Maroso M, Syage A, Allen BD, Angulo MC, Soltesz I, et al. Persistent nature of alterations in cognition and neuronal circuit excitability after exposure to simulated cosmic radiation in mice. Experimental neurology. 2018;305:44–55. Epub 2018/03/16. [PubMed: 29540322]
28. Leger M, Quiedeville A, Bouet V, Haelewyn B, Boulouard M, Schumann-Bard P, et al. Object recognition test in mice. Nature protocols. 2013;8(12):2531–7. Epub 2013/11/23. [PubMed: 24263092]
29. Zhao ZH, Zheng G, Wang T, Du KJ, Han X, Luo WJ, et al. Low-level Gestational Lead Exposure Alters Dendritic Spine Plasticity in the Hippocampus and Reduces Learning and Memory in Rats. Scientific reports. 2018;8(1):3533 Epub 2018/02/25. [PubMed: 29476096]
30. Mikolaenko I, Rao LM, Roberts RC, Kolb B, Jinnah HA. A Golgi study of neuronal architecture in a genetic mouse model for Lesch-Nyhan disease. Neurobiology of disease. 2005;20(2):479–90. Epub 2005/05/24. [PubMed: 15908225]
31. Groves TR, Wang J, Boerma M, Allen AR. Assessment of Hippocampal Dendritic Complexity in Aged Mice Using the Golgi-Cox Method. Journal of visualized experiments : JoVE. 2017(124). Epub 2017/07/04.
32. Sholl DA. Dendritic organization in the neurons of the visual and motor cortices of the cat. Journal of anatomy. 1953;87(4):387–406. Epub 1953/10/01. [PubMed: 13117757]
33. Morley BJ, Mervis RF. Dendritic spine alterations in the hippocampus and parietal cortex of alpha7 nicotinic acetylcholine receptor knockout mice. Neuroscience. 2013;233:54–63. Epub 2012/12/29. [PubMed: 23270857]
34. Titus AD, Shankaranarayana Rao BS, Harsha HN, Ramkumar K, Srikumar BN, Singh SB, et al. Hypobaric hypoxia-induced dendritic atrophy of hippocampal neurons is associated with cognitive impairment in adult rats. Neuroscience. 2007;145(1):265–78. Epub 2007/01/16. [PubMed: 17222983]

35. Magarinos AM, Li CJ, Gal Toth J, Bath KG, Jing D, Lee FS, et al. Effect of brain-derived neurotrophic factor haploinsufficiency on stress-induced remodeling of hippocampal neurons. Hippocampus. 2011;21(3):253–64. Epub 2010/01/23. [PubMed: 20095008]
36. Dellu F, Fauchey V, Le Moal M, Simon H. Extension of a new two-trial memory task in the rat: influence of environmental context on recognition processes. Neurobiology of learning and memory. 1997;67(2):112–20. Epub 1997/03/01. [PubMed: 9075239]
37. Burke SN, Wallace JL, Nematollahi S, Uprety AR, Barnes CA. Pattern separation deficits may contribute to age-associated recognition impairments. Behavioral neuroscience. 2010;124(5):559–73. Epub 2010/10/14. [PubMed: 20939657]
38. Cohen SJ, Stackman RW Jr. Assessing rodent hippocampal involvement in the novel object recognition task. A review. Behavioural brain research. 2015;285:105–17. Epub 2014/08/30. [PubMed: 25169255]
39. Neurobiology Eichenbaum H.. The topography of memory. Nature. 1999;402(6762):597–9. Epub 1999/12/22. [PubMed: 10604462]
40. Parihar VK, Allen BD, Tran KK, Chmielewski NN, Craver BM, Martirosian V, et al. Targeted overexpression of mitochondrial catalase prevents radiation-induced cognitive dysfunction. Antioxidants & redox signaling. 2015;22(1):78–91. Epub 2014/06/21. [PubMed: 24949841]
41. Raber J, Allen AR, Sharma S, Allen B, Rosi S, Olsen RH, et al. Effects of Proton and Combined Proton and (56)Fe Radiation on the Hippocampus. Radiation research. 2016;185(1):20–30. Epub 2016/01/01. [PubMed: 26720797]
42. Krukowski K, Feng X, Paladini MS, Chou A, Sacramento K, Grue K, et al. Temporary microglia-depletion after cosmic radiation modifies phagocytic activity and prevents cognitive deficits. Scientific reports. 2018;8(1):7857 Epub 2018/05/20. [PubMed: 29777152]
43. Hara Y, Waters EM, McEwen BS, Morrison JH. Estrogen Effects on Cognitive and Synaptic Health Over the Lifecourse. Physiological reviews. 2015;95(3):785–807. Epub 2015/06/26. [PubMed: 26109339]
44. Satterthwaite TD, Vandekar S, Wolf DH, Ruparel K, Roalf DR, Jackson C, et al. Sex differences in the effect of puberty on hippocampal morphology. Journal of the American Academy of Child and Adolescent Psychiatry. 2014;53(3):341–50 e1. Epub 2014/02/26. [PubMed: 24565361]
45. Qi X, Zhang K, Xu T, Yamaki VN, Wei Z, Huang M, et al. Sex Differences in Long-Term Potentiation at Temporoammonic-CA1 Synapses: Potential Implications for Memory Consolidation. PloS one. 2016;11(11):e0165891 Epub 2016/11/03. [PubMed: 27806108]
46. Villasana L, Rosenberg J, Raber J. Sex-dependent effects of 56Fe irradiation on contextual fear conditioning in C57BL/6J mice. Hippocampus. 2010;20(1):19–23. Epub 2009/06/03. [PubMed: 19489001]
47. Larkin MC, Lykken C, Tye LD, Wickelgren JG, Frank LM. Hippocampal output area CA1 broadcasts a generalized novelty signal during an object-place recognition task. Hippocampus. 2014;24(7):773–83. Epub 2014/03/07. [PubMed: 24596296]
48. Zheng C, Bieri KW, Hwaun E, Colgin LL. Fast Gamma Rhythms in the Hippocampus Promote Encoding of Novel Object-Place Pairings. eNeuro. 2016;3(2). Epub 2016/06/04.
49. Gu L, Kleiber S, Schmid L, Nebeling F, Chamoun M, Steffen J, et al. Long-term in vivo imaging of dendritic spines in the hippocampus reveals structural plasticity. The Journal of neuroscience : the official journal of the Society for Neuroscience. 2014;34(42):13948–53. Epub 2014/10/17. [PubMed: 25319691]
50. Tavosanis G Dendritic structural plasticity. Developmental neurobiology. 2012;72(1):73–86. Epub 2011/07/16. [PubMed: 21761575]
51. Moy SS, Nadler JJ, Perez A, Barbaro RP, Johns JM, Magnuson TR, et al. Sociability and preference for social novelty in five inbred strains: an approach to assess autistic-like behavior in mice. Genes, brain, and behavior. 2004;3(5):287–302. Epub 2004/09/04.
52. Morisot N, Monier R, Le Moine C, Millan MJ, Contarino A. CRF2 receptor-deficiency eliminates social behaviour deficits and vulnerability induced by cocaine. British journal of pharmacology. 2018 Epub 2018/02/07.

53. McKibben CE, Reynolds GP, Jenkins TA. Analysis of sociability and preference for social novelty in the acute and subchronic phencyclidine rat. Journal of psychopharmacology. 2014;28(10):955–63. Epub 2014/08/15. [PubMed: 25122039]
54. Castelhano AS, Cassane Gdos S, Scorza FA, Cysneiros RM. Altered anxiety-related and abnormal social behaviors in rats exposed to early life seizures. Frontiers in behavioral neuroscience. 2013;7:36 Epub 2013/05/16. [PubMed: 23675329]
55. Felix-Ortiz AC, Tye KM. Amygdala inputs to the ventral hippocampus bidirectionally modulate social behavior. The Journal of neuroscience : the official journal of the Society for Neuroscience. 2014;34(2):586–95. Epub 2014/01/10. [PubMed: 24403157]
56. Hitti FL, Siegelbaum SA. The hippocampal CA2 region is essential for social memory. Nature. 2014;508(7494):88–92. Epub 2014/02/28. [PubMed: 24572357]
57. Chiang MC, Huang AJY, Wintzer ME, Ohshima T, McHugh TJ. A role for CA3 in social recognition memory. Behavioural brain research. 2018 Epub 2018/01/23.
58. Kohara K, Pignatelli M, Rivest AJ, Jung HY, Kitamura T, Suh J, et al. Cell type-specific genetic and optogenetic tools reveal hippocampal CA2 circuits. Nature neuroscience. 2014;17(2):269–79. Epub 2013/12/18. [PubMed: 24336151]
59. Chevaleyre V, Siegelbaum SA. Strong CA2 pyramidal neuron synapses define a powerful disynaptic cortico-hippocampal loop. Neuron. 2010;66(4):560–72. Epub 2010/06/01. [PubMed: 20510860]
60. Mohedano-Moriano A, Pro-Sistiaga P, Ubeda-Banon I, Crespo C, Insausti R, Martinez-Marcos A. Segregated pathways to the vomeronasal amygdala: differential projections from the anterior and posterior divisions of the accessory olfactory bulb. The European journal of neuroscience. 2007;25(7):2065–80. Epub 2007/04/11. [PubMed: 17419754]
61. Brennan PA, Kendrick KM. Mammalian social odours: attraction and individual recognition. Philosophical transactions of the Royal Society of London Series B, Biological sciences. 2006;361(1476):2061–78. Epub 2006/11/23. [PubMed: 17118924]
62. Risold PY, Swanson LW. Connections of the rat lateral septal complex. Brain research Brain research reviews. 1997;24(2–3):115–95. Epub 1997/12/31. [PubMed: 9385454]
63. Luscher Dias T, Fernandes Golino H, Moura de Oliveira VE, Dutra Moraes MF, Schenatto Pereira G. c-Fos expression predicts long-term social memory retrieval in mice. Behavioural brain research. 2016;313:260–71. Epub 2016/07/28. [PubMed: 27449201]

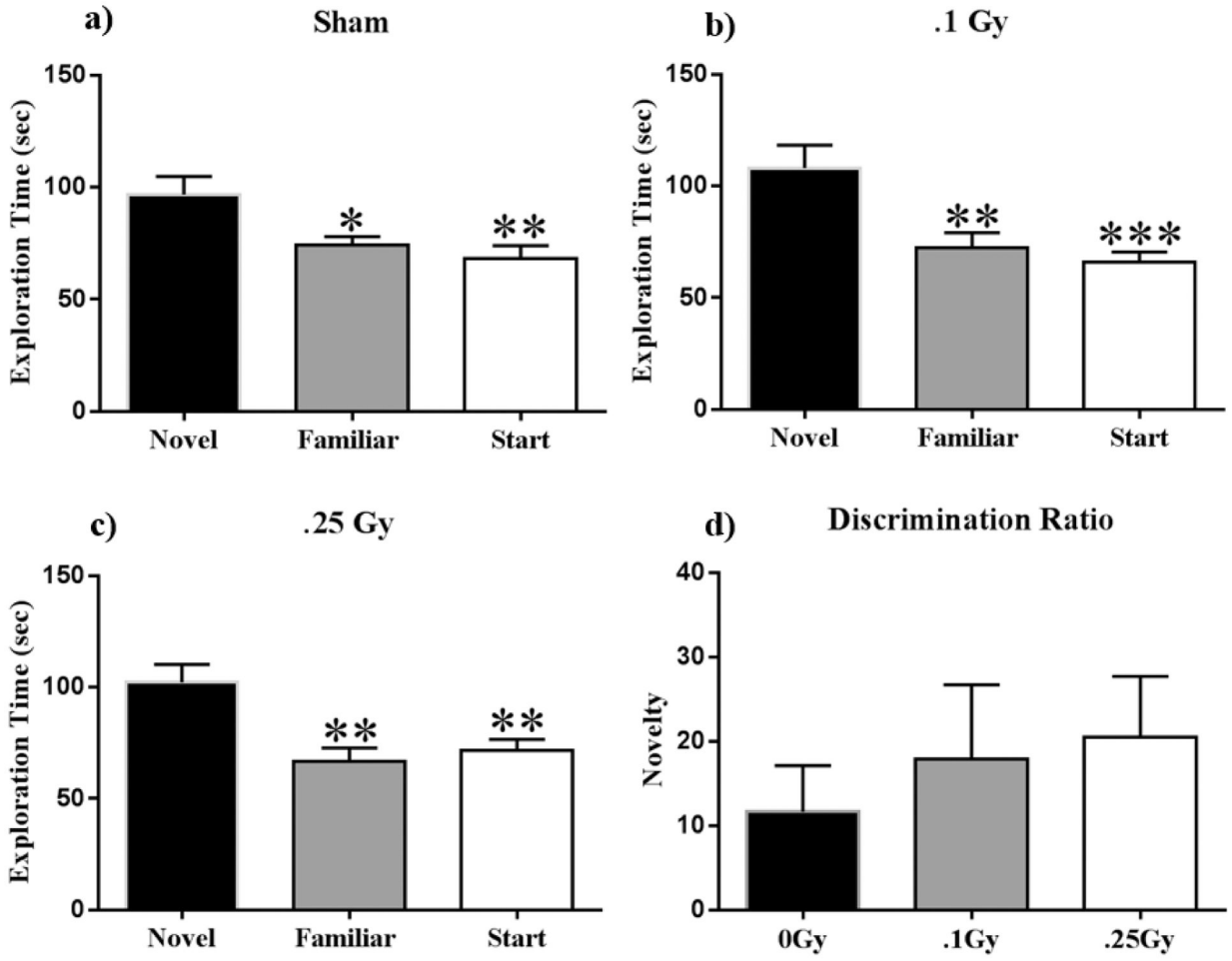

Figure 1: Y-maze.

(A-C) All treatment groups spent significantly more time exploring the novel arm during the testing phase of the Y-maze, indicating no short-term memory deficits. 2. **D)** All cohorts showed positive discrimination ratios with no significant differences, and thus displayed similar novelty discrimination in all groups. Average ± SEM (n = 12); $*P < 0.05$, $**P < 0.01$, $***P < 0.001$.

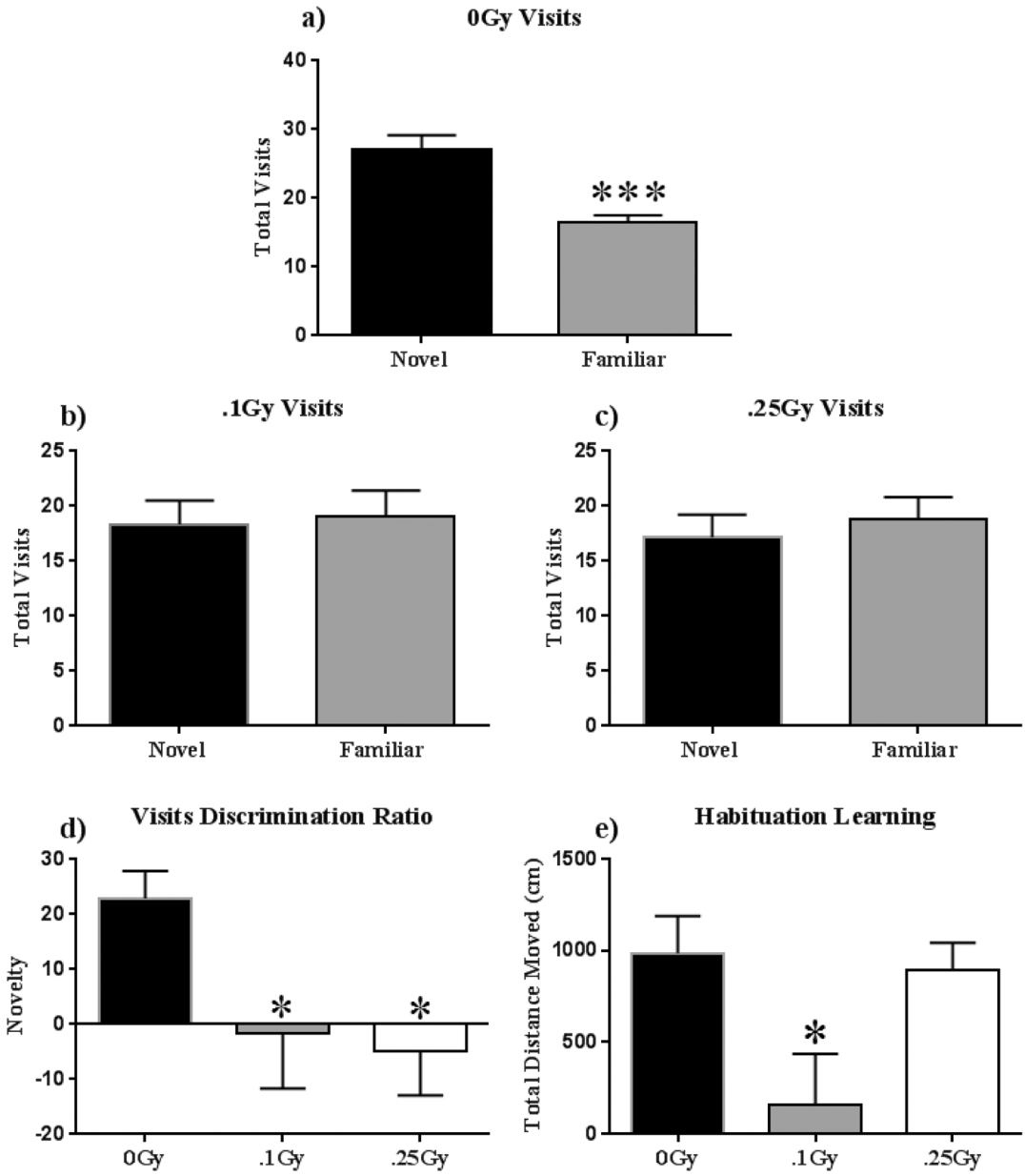

Figure 2: Novel Object Recognition.

(A-C) Both irradiated groups were unable to discern the novel from the familiar object on test day, whereas sham-irradiated animals spent significantly more time exploring the novel object. **(D)** Radiation induced negative discrimination ratios, representing an inability to discriminate between the novel and familiar objects. **(E)** Animals who received 0.1 Gy displayed very low habituation as compared other cohorts on habituation day 2. Average ± SEM (n = 12); $*P < 0.05$, $***P < 0.001$.

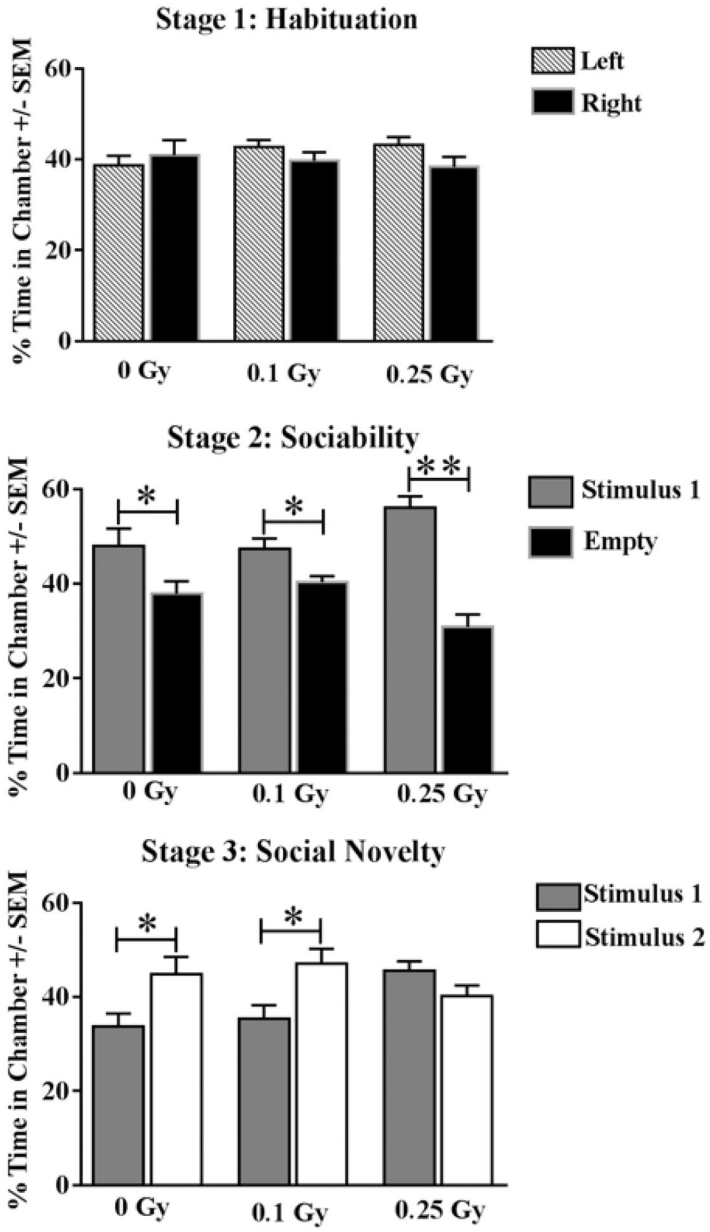

Figure 3: Sociability.

(A) Animals of all cohorts displayed no significant chamber-exploration bias. **(B)** All cohorts displayed normal sociability by spending significantly more time with a novel mouse (stimulus 1). **(C)** Sham-irradiated and mice receiving 0.1 Gy were able to discriminate between a novel stranger (Stimulus 2), and a now-familiar stranger (Stimulus 1), whereas mice treated with 0.25 Gy failed to distinguish strangers. Average ± SEM (n = 12); $*P < 0.05$, $**P < 0.0001$.

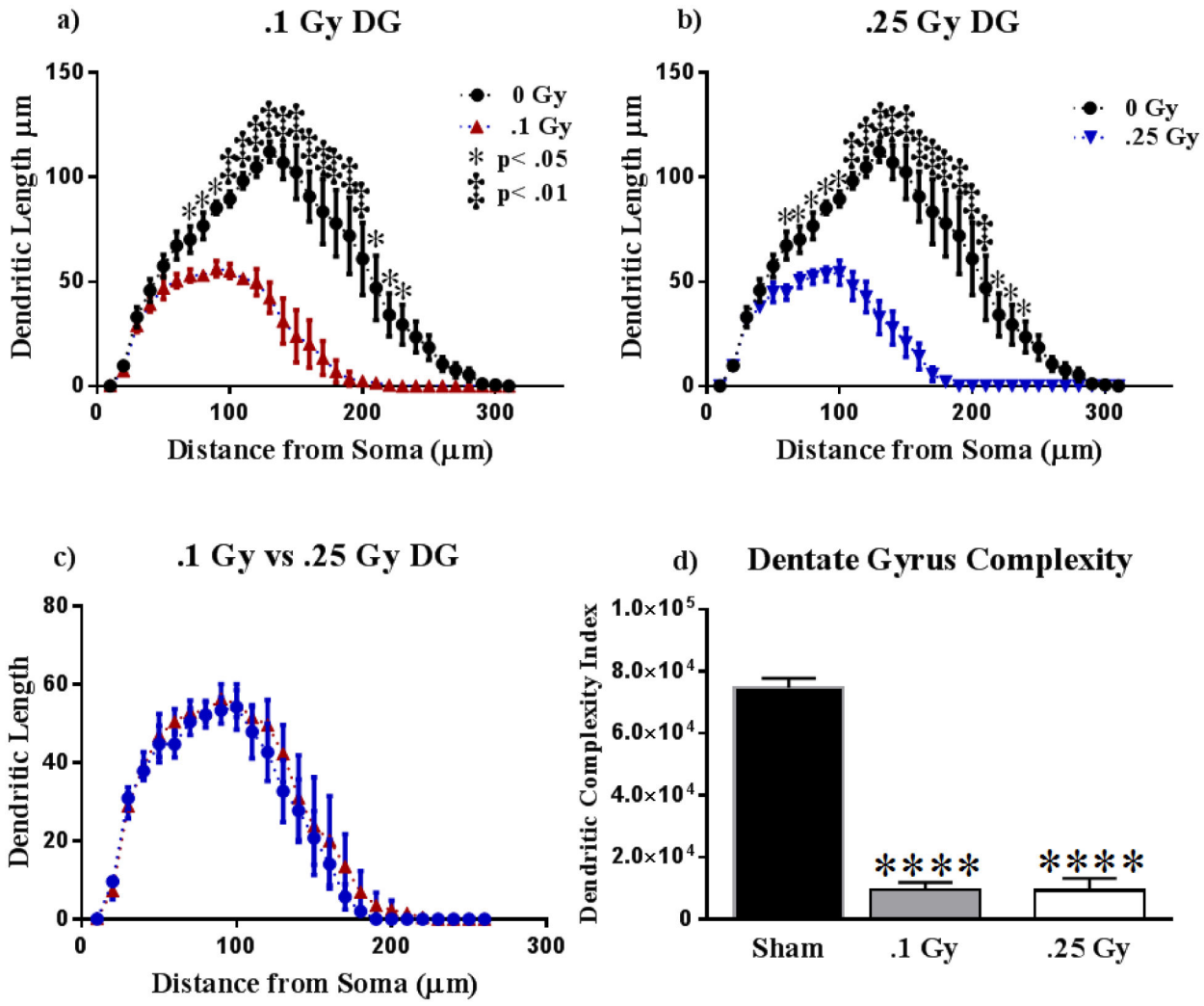

Figure 4: Dentate Gyrus Dendrite Morphology.

(A-B) Dendritic length reduces significantly due to 0.1 and 0.25 Gy of 16O. **(C)** Irradiation resulted in nearly identical dendritic reductions in the mossy fibers of the dorsal Dentate Gyrus. **(D)** Dendritic complexity is severely reduced at both radiation dosages. Average ± SEM (n = 5); ****$P < 0.0001$.

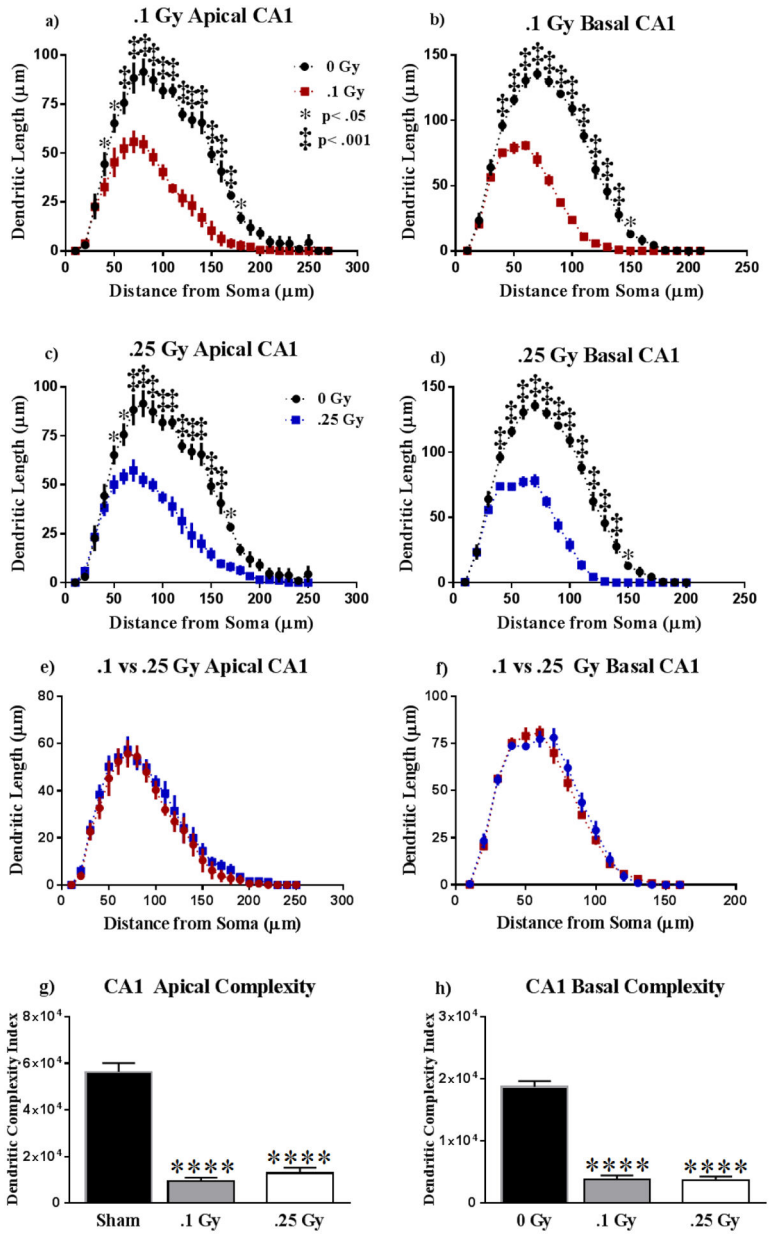

Figure 5: Dorsal CA1 Dendritic Morphology.

(A-D) The apical and basal CA1 underwent significant reduction in dendritic length beginning at approximately 50 µm from the soma. **(E-F)** The extent of dendritic remodeling appears to be dosage independent. **(G-H)** Dendritic complexity was significantly lowered as a result of treatment, in dosage-independent manner. Average ± SEM (n = 5); ****$P <$ 0.0001.

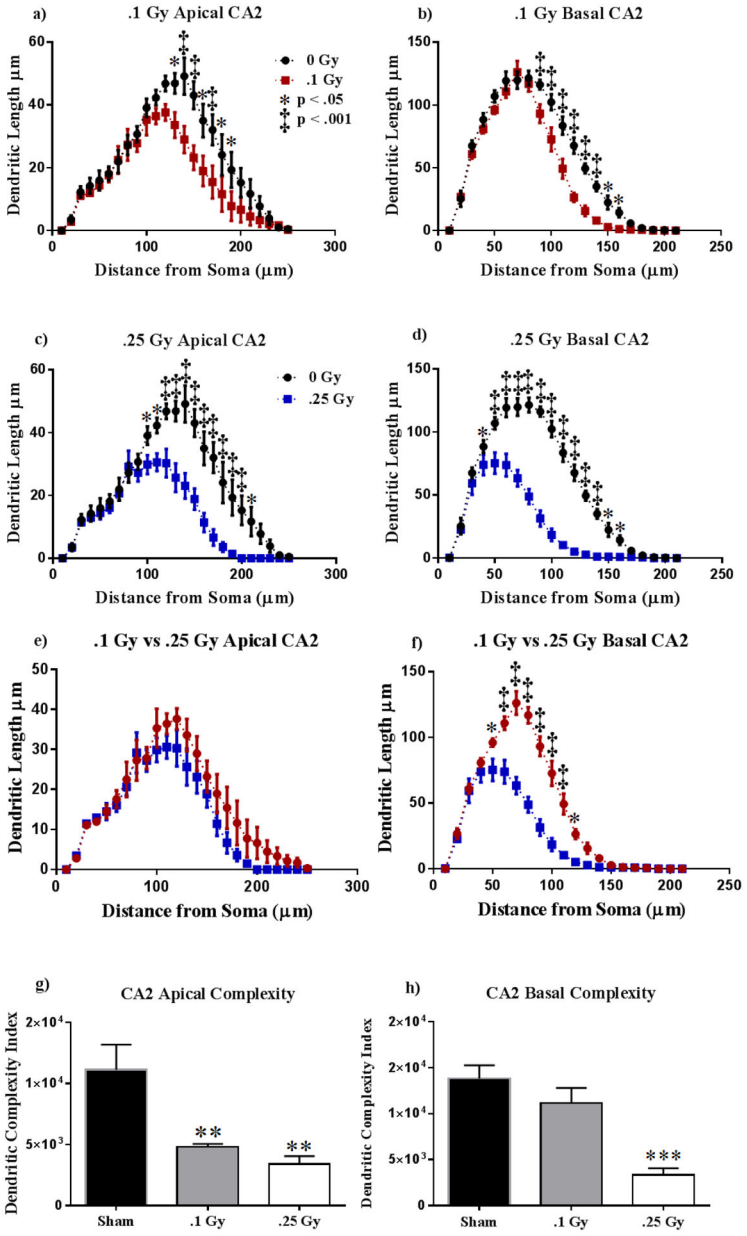

Figure 6: Dorsal CA2 Dendritic Morphology.

(A-D) Animals irradiated at 0.1 Gy or 0.25 Gy suffered a decrease in dendritic length in both apical and basal dendrites. **(E-F)** Radiation dosage resulted in generally indistinguishable dendritic reduction in the apical CA2, but a dosage of 0.25 Gy resulted in significantly higher dendritic length reduction. **(G-H)** Apical complexity was reduced in both treatment groups, whereas only the higher dosage lowered basal dendritic complexity. Average ± SEM (n = 5); $*P < 0.05$, $**P < 0.01$, $***P < 0.001$.

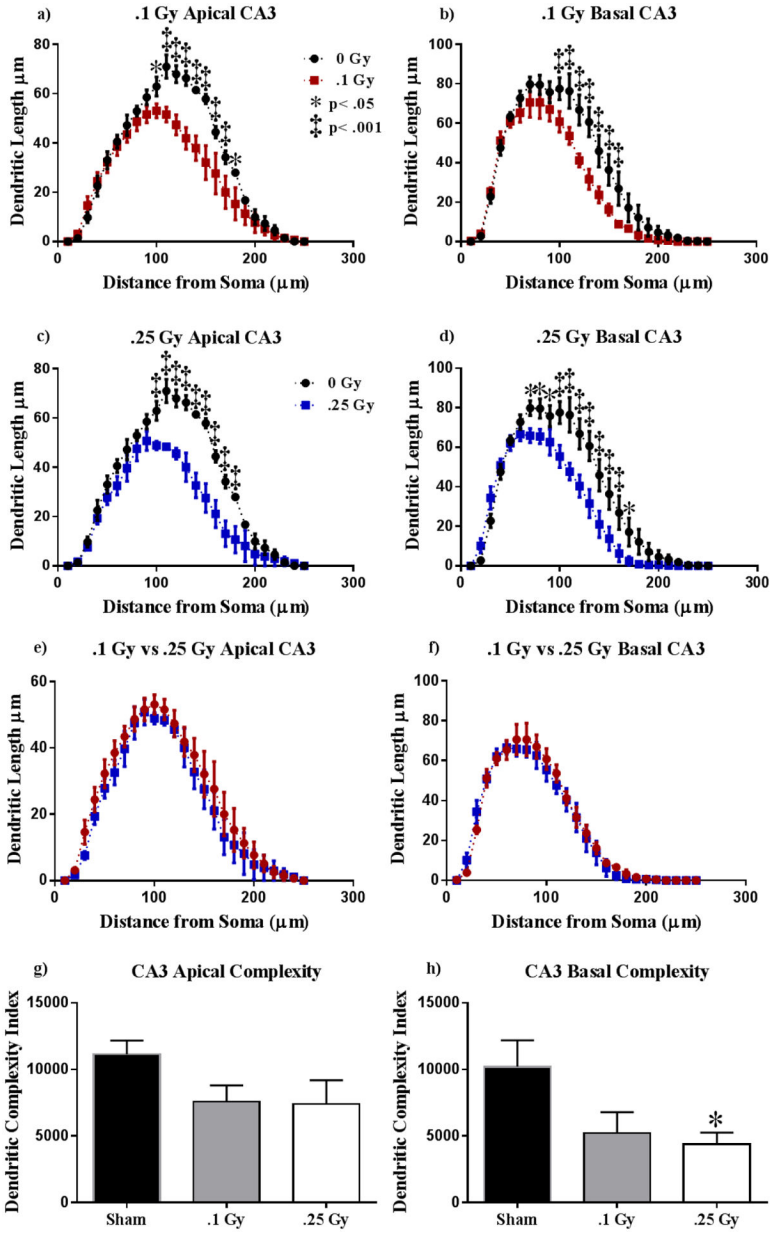

Figure 7: Ventral CA3 Dendritic Morphology.

(A-B) A dosage of 0.1 Gy elicited dendritic length reductions at approximately 100–160 µm from the soma in both the basal and apical CA3. **(C-D)** Dendritic length decreases in response to a dosage of 0.25 Gy. **(E-F)** Radiation at the dosages of 0.1 and 0.25 Gy induces nearly identical dendritic reduction in the apical and basal CA3. (**G-H**) Dendritic complexity is only significantly reduced in the basal CA3 at 0.25 Gy. Average ± SEM (n = 5); **P* < 0.05.

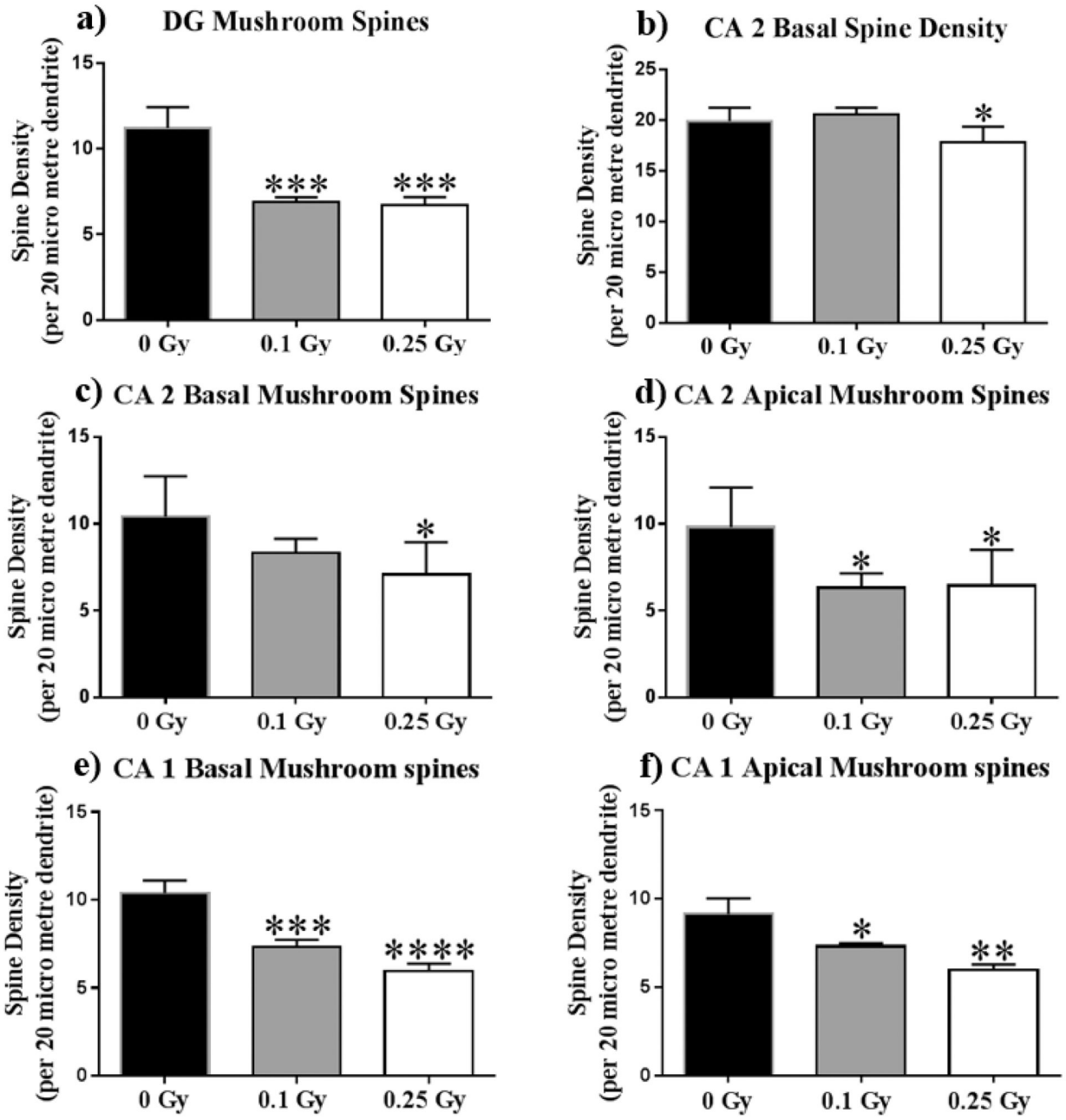

Figure 8: ^{16}O reduces mushroom spine density in the hippocampus.

(A) Dentate Gyrus mushroom spine density lowers by about one third in irradiated animals. **(C)** The Apical CA2 underwent reduced mushroom spine density in both dosages. (**B,D**) The basal CA2 overall, and mushroom spine density at only 0.25 Gy. (**E,F**) Apical and basal CA1 mushroom spines decrease in a dose-dependent manner in irradiated animals. Average ± SEM (n = 5); *$P < 0.05$, **$P < 0.01$, ***$P < 0.001$, ****$P < 0.0001$.

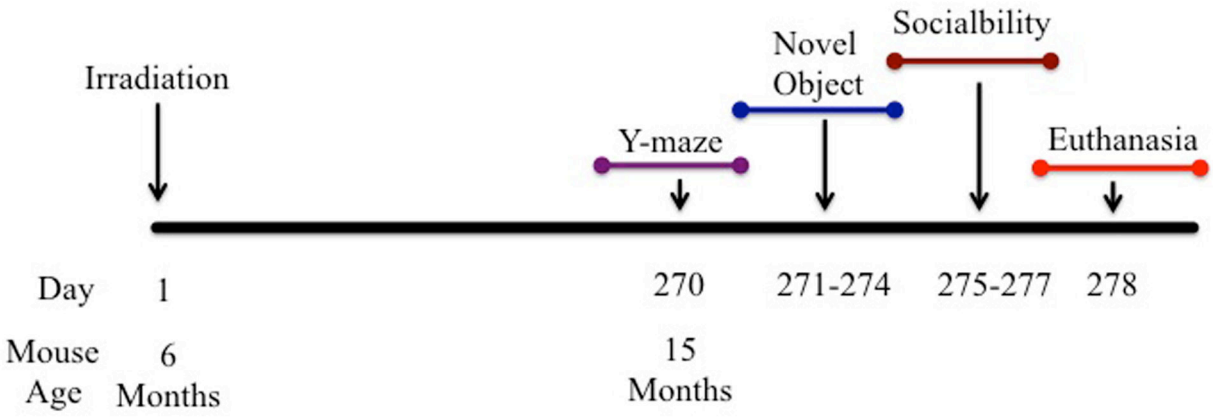

Schematic diagram showing experimental design.

Six-month-old C57BL/6J Female mice received whole-body irradiation ^{16}O radiation at doses of 0, 0.1 or 0.25 Gy (600MeV/n) at NASA's Space Radiation Laboratory (NSRL) within BNL. 270 Days post irradiation behavioral testing was performed.

Table 1:

Effects of ^{16}O on Dendrite Morphology in the DG

Cell Type and Measurement	0 Gy (menu ± SEM)	.5 Gy (menu ± SEM)	1 Gy (mean ± SEM)
DG			
Total Dendritic Length (μm)	1225 ± 41.17	*478.5 ± 69.91*	*482.9 ± 43.88*
Total # Branch Points	11.20 ± 0.41	*4.06 ± 0.37*	*4.10 ± 0.33*
Dendritic Ends	12.65 ± 0.43	*5.63 ± 0.48*	*5.40 ± 0.37*
Cell Area	191.5 ± 21.19	218.7 ± 65.40	187.5 ± 13.36

Table 2:

Effects of ^{16}O on Dendrite Morphology in the CA1

Cell Type and Measurement	0 Gy (mean ± SEM)	0.1 Gy (mean ± SEM)	0.25 Gv (mean ± SEM)
CA1 Apical			
Total Dendntic Length (μm)	1091 ± 129	*429.3 ± 23.84*	*506.6 ± 44.41*
Total # Branch Points	8.96 ± 0 46	*4.36 ± 0.36*	*4.72 ± 0.35*
Dendntic Ends	9.96 ± 0.46	*5.48 ± 0.40*	*5.76 ± 0.38*
CA1 Basal			
Total Dendritic Length (μm)	465.7 ± 33.34	*198.2 ± 17.58*	*200.1 ± 21.97*
Total # Branch Points	9.39 ± 0 24	*3.92 ± 0.29*	*3.88 ± 0.39*
Dendntic Ends	7.00 ± 0.26	6.76 ±0.33	*12.35 ± 0.28*
CA1 Cell Area	233.2 ± 26.04	199.9 ± 16 09	242.4 ± 20.24

Table 3:

Effects of ^{16}O on Dendrite Morphology in the CA2

Cell Type and Measurement	0 Gy (mean ± SEM)	0.1 Gy (mean ± SEM)	0.25 Gv (mean ± SEM)
CA2 Apical			
Total Dendritic Length (μm)	562.7 ± 33.66	*403.4 ± 23.16*	*321.8 ± 20.37*
Total # Branch Points	3.75 ± 0.13	*2.70 ± 0.06*	*2.05 ± 0.13*
Dendritic Ends	4.80 ± 0.14	*3.70 ± 0.06*	*3.10 ± 0.10*
CA2 Basal			
Total Dendritic Length (μm)	1150 ± 46.17	*835.9 ± 6.23*	*486.6 ± 50.36*
Total # Branch Points	7.88 ± 0.31	6.95 ± 0.13	*3.58 ± 0.65*
Dendritic Ends	11.48 ± 0.59	10.16 ± 0.21	*6.45 ± 0.82*
CA2 Cell Area	239.8 ± 20.50	219.7 ± 27.72	264.7 ± 11.97

Table 4:

Effects of ^{16}O on Dendrite Morphology in the CA3

Cell Type and Measurement	0 Gy (mean ± SEM)	0.1 Gy (mean ± SEM)	0.25 Gy (mean ± SEM)
CA3 Apical			
Total Dendritic Length (μm)	800.8 ± 16.07	*612.4 ± 54.75*	*496.9 ± 23.63*
Total # Branch Points	4.60 ± 0.26	*3.44 ± 0.24*	*3.57 ± 0.31*
Dendritic Ends	6.32 ± 0.27	*4.80 ± 0.34*	*4.90 ± 0.29*
CA3 Basal			
Total Dendritic Length (μm)	912.6 ± 70 74	*664.3 ± 52.30*	*639.3 ± 39.90*
Total # Branch Points	5.55 ± 0.15	*3.64 ± 0.47*	*3.22 ± 0.43*
Dendritic Ends	7.84 ± 0.30	6.64 ± 0.52	*6.16 ± 0.35*
CA3 Cell Area	431.7 ± 47.55	447.7 ± 32.17	471.2 ± 8 95